Superhydrophobic flow channel surface and its impact on PEM fuel cell performance

Yongxin Wang[1,2], Saher Al Shakhshir[2], Xianguo Li[2*] and Pu Chen[1]
[1]*Department of Chemical Engineering;* [2]*Department of Mechanical and Mechatronics Engineering, University of Waterloo, Waterloo, ON, Canada N2L 3G1*

Abstract

Water management is a critical issue in polymer electrolyte membrane fuel cells (PEMFCs), and it is normally achieved through the modification of surface wettability condition for the cell components. In this study, superhydrophobic surface-coating materials were developed and the gas flow channel surfaces were modified for superhydrophobic surface property with small sliding angles (SAs). The coated surface characteristics were measured, including static contact angle (CA), SA and CA hysteresis as well as surface geometrical properties. The flow characteristics through such surface-coated channels were measured, and comparison was made with hydrophilic channels and channels coated with poly(tetrafluoroethylene), a commonly used surface-coating agent in PEMFCs. It was found that the presently modified superhydrophobic flow channels yield the lowest resistance to the two-phase flow; and both the mechanical and thermal stabilities of the attained superhydrophobicity for the coated surfaces were also investigated. It was demonstrated experimentally that such coated flow channels result in improved PEMFC performance due to improved water management.

Keywords: polymer electrolyte membrane fuel cell; water management; gas flow channel; surface wettability; superhydrophobicity; surface coating

*Corresponding author:
x6li@uwaterloo.ca

Received 27 March 2012; revised 22 June 2012; accepted 7 September 2012

1 INTRODUCTION

Hydrogen-fuelled polymer electrolyte membrane fuel cell (PEMFC) is considered one of the most promising zero-emission power sources for mobile, stationary and portable applications. One of the key technical barriers hindering the PEMFC commercialization is water management, which is a critical issue in PEMFCs [1, 2]. Excess liquid water accumulated in the gas distribution layer (GDL) and gas flow channels will lead to oxidant starvation and performance degradation [3]. In the past decades, water management within different components of fuel cells has been widely studied [4–7], particularly within the GDL [8], but the studies on gas flow channels are relatively limited [9–11]. The reaction product water formed inside the PEMFCs is normally removed through the reactant gas streams in the gas flow channels built on the bipolar plates. Furthermore, water vapour will condense on the flow channel surfaces due to the cooling arrangement in a PEMFC stack. Liquid water is difficult to be removed from the untreated flow channels by the reactant gas streams. Much more water will influence the function of GDL, significantly hindering the cell performance [8, 12–15].

One of the relatively straight techniques for the water removal from the flow channels is to change the channel surface wettability (such as static contact angle (CA) and sliding angle (SA) of water) to facilitate the liquid water mobility in the channel. One approach that has been suggested is to coat the channels with hydrophilic materials so that the removal of condensed water can be increased by fast evaporation [14, 16]. Extrand calculated the cross-sectional area of small sessile drops on solid surfaces with a wide range of wettability and investigated the relationship between static CA and blockage in small channels [17]. It was suggested in that work that even a small decrease of water CA, i.e. $<45^{\circ}$, will lead to a substantial decrease in the blockage of the channels. However, this conclusion is generally valid under low power conditions of a fuel cell. When quantities of water are produced under high power conditions, water flow, but not water droplet any more, will be formed. The help of water evaporation on its removal will be lower. A second approach to adjust the surface wettability

International Journal of Low-Carbon Technologies 2014, 9, 225–236

doi:10.1093/ijlct/cts069 Advance Access Publication 1 November 2012

condition is to coat the channels with hydrophobic materials so that the condensed water cannot stick in the channels, and can be effectively driven off the channels by the gas stream.

A number of techniques have been developed to prepare superhydrophobic surfaces, which are characterized by a high static CA of water, $>150^\circ$, and a small SA, $<10^\circ$ [16,18–22]. The SA refers to the tilting angle of a solid surface when the droplet starts sliding downwards. It is an important parameter to describe the water movability on a solid surface. The general approach to preparing a superhydrophobic surface requires the combination between the low surface energy coating and appropriate surface roughness [16,18–24]. In terms of low surface energy materials, poly(tetrafluoroethylene) (PTFE) is a typical material used for water-repellent coatings in PEMFCs [25]. However, the high cost and health hazard concerns hinder its commercial use [26]. Poly(dimethylsiloxane) (PDMS) is another commonly used material [27, 28]. Its good flexibility, transparency, thermal stability as well as non-toxicity make it a good candidate as a coating material.

Roughness plays an important role in determining the surface wettability of solids. The increasing surface roughness of hydrophobic materials can dramatically enhance its surface hydrophobicity [29–33]. Many theories including those of Wenzel, Cassie–Baxter have been developed to explain this phenomenon [32–36]. In general, an appropriate surface roughness should be constructed so that sufficient air (hydrophobic media) could be trapped on the surface [37]. Rough surfaces could be prepared by two approaches: one is to fabricate new rough structures on flat substrates and the second is to adjust the roughness of an existing rough surface. For the former approach, new rough surfaces can be fabricated by both chemical and physical methods such as wax solidification [38, 39], sol–gel processing [40, 41], lithography [42, 43] and vapour deposition [44–47]. In contrast, the second approach has been less studied. Graphite, conventionally used as bipolar plate materials for PEMFCs, has a rough surface [48]. The porosity is 18–32% for a typical graphite plate [49]. The static water CA is around 95° on an untreated graphite surface. Water droplets usually stick on this surface, and are difficult to be removed even by a relatively strong air flow. Mench *et al.* [27] applied PTFE to coat the graphite bipolar plate, resulting in a static CA of 108° on the coated surface. PTFE reduces the surface energy of graphite, rendering a water repellent surface. However, towards attaining a high water-repellent surface of graphite, the adjustment of its surface roughness should also be considered. Yasuda *et al.* pretreated the gas flow channel using a sand-blast method to adjust its surface roughness, and then coated it with PTFE by plasma polymerization. The measured water CA was about 135°, which was better than the surface treated by plasma polymerization without the sand-blast pretreatment [50]. However, a graphite channel with only a high water CA is not enough to drain off the condensed water effectively. In an ideal hydrophobic channel, the SA should also be as low as possible. As shown above, many studies have been carried out to increase the surface CAs, and the significance of the SA reduction has not been paid appropriate attention by the PEMFC community.

In this study, the main objective was to create a superhydrophobic surface for flow channels on the bipolar plates with small SAs for improved water removal. The surface of graphite was coated by using a silica particle/PDMS composite, where silica particles ranging from nano to micro sizes were employed to adjust the surface roughness of graphite and PDMS served as a low surface energy material. The movement of a water droplet in a superhydrophobic graphite channel, which was coated with the silica particle/PDMS composite, was compared with that in a superhydrophilic graphite channel, which was coated with silica particles. In addition, the thermal and mechanical stabilities of the resulting surfaces were investigated. Finally, single-cell tests confirm that PEMFCs with superhydrophobic flow channel surfaces (especially with small SAs) yield an improved PEMFC performance due to the improved water removal capability.

2 EXPERIMENTAL

2.1 Materials

A fuel cell-grade graphite bipolar plate was cut into square samples (20×20 mm) and channels ($150 \times 4 \times 4$ mm, channel size). All these samples were cleaned by ultrasound to wash off the absorbed carbon powders. Tetramethyl orthosilicate (TEOS), ammonium hydroxide aqueous solution (28.0–30.0 wt%) and PTFE (60 wt% in H_2O) were purchased from Sigma-Aldrich Ltd., ON, Canada. Hydroxyl-terminated PDMS (PDMS-1, 750 cst) was purchased from Gelest Inc., PA, USA. The Sylgard 184 kit (PDMS-2), containing PDMS oligomers and curing agents, was purchased from Dow Corning, MI, USA. The solvents, such as ethanol, methanol, isopropanol and tetrahydrofuran (THF), were of analytical grade and used as received from Sigma-Aldrich Ltd. The water used was prepared using Milli-Q Ultrapure Water system (Millipore Co., Billerica, MA, USA).

2.2 Synthesis of silica particles

Silica particles were prepared by employing the modified Stöber method [51, 52]. The formulation was listed in Table 1. Ethanol (or other alcohols) and ammonia were mixed together under the protection of N_2; TEOS was then added dropwise for 15 min. The system was allowed to react overnight at room temperature and under N_2. Ammonia was removed by rotary evaporation. The particles were separated by centrifugation and washed by Milli-Q water.

Table 1. *Formulation for the synthesis of silica particles.*

No. of formulation	1	2	3	4	5
Ammonia (ml)	6	14	18	20	10
TEOS (ml)	6	6	6	6	5
Ethanol (ml)	200	200	200	200	–
Methanol + isopropanol (ml)	–		–	–	12.5 + 37.5

The prepared silica particles were dispersed in ethanol, and their size and size distribution (polydispersity index, PDI) were measured by dynamic light scattering (Zetasizer, Malvern Inc., UK) at 20°C. The PDI is calculated from the equation: $\ln(G1) = a + bt + ct^2 + dt^3$, where $G1$ is a correlation function. The second-order cumulant b is known as the z-average diffusion coefficient [53]. The coefficient of the squared term c, when scaled as $2c/b^2$, is defined as PDI, which can range from 0 (monodisperse) to 1 (polydisperse). The Z-average diameter of silica particles prepared from the formulation of No. 1 in Table 1 is 72 nm and PDI is 0.187; for No. 2 is 262 nm and PDI is 0.02; for No. 3 is 510 nm and PDI is 0.332; for No. 4 is 745 nm and PDI is 0. 201; and for No. 5 is 1.139 μm and PDI is 0.887.

Silica particles of size 262 nm were also coated on the graphite channel to obtain the hydrophilic channel. Silica particles with an average size of 262 nm (1 wt%) were dispersed in THF by ultrasound. 0.5 ml of this mixture was evenly brushed on the graphite channel (150 × 4 × 4 mm). After the solvent evaporated, the channel was heated for 5 min at 180°C.

2.3 Preparation of PDMS and PTFE coatings on graphite

Two kinds of silicone materials, hydroxyl-terminated PDMS (PDMS-1) and Dow Corning Sylgard 184 (PDMS-2), were applied to coat graphite, separately. Each of them was dissolved in THF, resulting into 1 wt% solution. 0.04 ml of the solution was spread on the graphite and cured at 180°C. PDMS-1 required 30 min to be completely cured while PDMS-2 was cured in 5 min. As for PTFE, 60 wt% PTFE emulsion was diluted to 15 wt%. 0.04 ml of this emulsion was spread on the graphite (20 × 20 mm) and cured at an ambient condition for 3 h. After that, the surface was washed thoroughly by methanol to remove the surfactants from the emulsion.

PTFE was also coated on the graphite channel. The 60 wt% PTFE emulsion was diluted to 15 wt%. 0.5 ml of this emulsion was brushed over the graphite channel (150 × 4 × 4 mm) and cured at an ambient condition for 3 h.

2.4 Preparation of silica particle/PDMS composite coatings on graphite

Prepared silica particles of each size (72–1139 nm, 1 wt%) and PDMS-1 (or PDMS-2) (1 wt%) were dispersed in THF by ultrasound. 0.04 ml of this mixture was evenly spread on the surface of graphite (20 × 20 mm). When the solvent evaporated, the sample was heated for 30 min for silica particle/PDMS-1 composite coating and for 5 min for silica particle/PDMS-2 composite coating at 180°C.

262 nm-sized silica particle/PDMS-2 composite was also coated on the graphite channel. Silica particles with an average size of 262 nm (1 wt%) and PDMS-2 (1 wt%) were dispersed in THF by ultrasound. 0.5 ml of this mixture was evenly brushed on the graphite channel (150 × 4 × 4 mm). When the solvent evaporated, the channel was heated for 5 min at 180°C.

2.5 Characterization

The surface topography of the coated graphite was observed by a field-emission scanning electron microscope (SEM) (LEO 1530, Germany), and the surface roughness was measured on Optical Profiler (WYKO NT1100, USA). Surface static CA, SA as well as dynamic CA of water were tested on Axisymmetric Drop Shape Analysis-Profile (ADSA-P) [54], where a PTFE needle (inner diameter 0.25 mm; outer diameter 0.52 mm) was used to inject small volume (10 μl) of water droplets. For each kind of samples, 3 parallel samples were prepared, 10 different locations were tested on each of them and standard deviation was calculated. During the tests, 10 μl of Milli-Q water droplets were used for CA and SA; all of the CAs were measured by the ellipse fitting method [55–57].

Figure 1 illustrates the experimental setup used for measuring the pressure drop through the graphite channel and visualizing the air/water two-phase flow inside the graphite channel. The flow rate of the water and air is measured by the respective flowmeters, and the pressure difference between the inlet and exit of the flow channel is measured by a pressure gauge. The two-phase flow behaviour inside the flow channel is observed through the transparent top cover made of plexiglass. The cross section of the water inlet was circular with a diameter of 0.5 mm. The cross section of the air inlet was circular with a diameter of 2 mm. During the test, the superficial velocity of water was fixed at 0.015 m/s, and the flow rate of air was controlled by an air flow meter. The superficial velocity was calculated by the measured flow rate divided by the cross-sectional area of the channel, which is 4 × 4 mm. A high-speed complementary metal oxide semiconductor (CMOS) camera system was used to record the air/water flow behaviour inside the channel.

A PEMFC was designed and built with a 43 cm^2 active area. All membrane electrode assemblies contain Nafion® 112, the catalyst loading of 0.5 mg cm^{-2} Pt/C for both cathode and anode, and the GDL (provided by SolviCore Fuel Cell Technology, Germany). The GDL has a microporous layer. Two kinds of graphite bipolar plates (dimension 135 × 35 mm), raw one (flow channel surfaces are not coated) and the one with channels coated with 262 nm silica particle/PDMS-2 composite, were used in the single-cell performance testing. On both of these bipolar plates, serpentine-type flow channels were machined with a 3 × 3 mm gas-channel cross-sectional area. The clamping force to assemble the fuel cell was 53.4 kN. The fuel cell test system (FCATS, Hydrogenics Inc.) used in the experiment consisted of a gas sub-system, electronic load box and a computer running a controlling and data-logging software (HyWare®) for the automatic control. All the performance tests were conducted under the same conditions: cell operating temperature of 65°C, relative humidity of 100% for both hydrogen and air streams, inlet pressure of 100 kPag at the anode and cathode inlets and the stoichiometric ratio of 2 for O_2 in air and 1.2 for H_2. During the cell performance test, the cell was initially set at a fixed operating current density, typically at 25 mA/cm^2; after the cell reached the steady state,

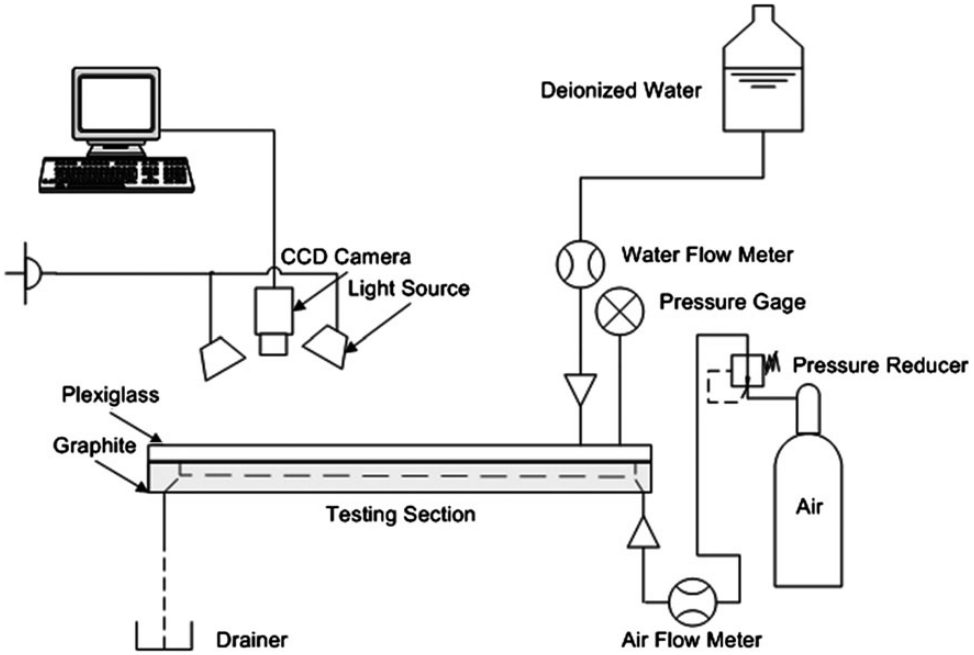

Figure 1. *Schematic of the experimental setup for the characterization of two-phase flow through the coated graphite channel.*

the cell was run in a load—following forward sweeping mode from 50 to 1500 mA/cm^2. The sweep step was 50 mA/cm^2, and each reading was recorded after 200 s of the current loading change since 200 s was sufficient for the cell performance to reach steady state after each step change of the current density.

3 RESULTS AND DISCUSSION

3.1 Hydrophilic coating on graphite surface with silica particles

As mentioned earlier, hydrophilic coating can also improve the water removal by increased evaporation. In the present work, hydrophilic coating is prepared on graphite by silica particles, which are typically hydrophilic with the surface hydroxyl groups [58]. Silica particles of five sizes, 72, 262, 510, 745 nm and 1.139 μm, are prepared. The non-coated graphite is slightly hydrophobic with a static water CA of 95 ± 2° (Table 2). Water droplets (10 μl) generally stick on the surface and cannot slide downwards by gravity even if the surface is tilted over 90°. However, as graphite is coated with silica particles of size 72 nm, the water CA decreases sharply to about 15° (Table 2). The hydrophilic surfaces are also attained with graphite coated with silica particles of other sizes. Additionally, it was found when a water droplet touched the coated surface; it could spread over the surface gradually. For example, the initial water CA was about 60° on the graphite coated with 262 nm-sized silica particles, then the CA decreased gradually to about 30° in 2 min. This phenomenon cannot be observed with non-coated graphite.

Table 2. *Water CAs measured for graphite surfaces coated by silica particles*[a].

Particle size (nm)	0[b]	72	262	510	745	1139
CA	95 ± 2°	15 ± 2°	35 ± 2°	32 ± 3°	34 ± 2°	35 ± 5°

[a]10 μl of Milli-Q water droplet was used for each water CA measurement, and all the values were measured 2 min after the water droplet was placed on the surface.

[b]Particle size 0 means the original raw graphite surface.

3.2 Hydrophobic coatings on the graphite surface with PTFE and PDMS

As pointed out earlier, low surface energy materials can help to prepare a water repellent surface through appropriate surface coatings. In this work, PTFE and PDMS are used as the low surface energy coating materials to coat the graphite. Here two kinds of PDMS, hydroxyl-terminated PDMS (PDMS-1) and Sylgard 184 (PDMS-2), are applied. Statistically, the same CA and SA results were obtained for both PDMS-1- and PDMS-2-coated surfaces (Table 3). The highest static CA on PTFE-coated graphite is 145 ± 5° and SA is 48 ± 3°, whereas the highest CA on PDMS-coated graphite is 145 ± 5° and SA is 45 ± 5°. The CA values are larger than those on a flat, pure PTFE surface (CA = 120°) and a pure PDMS surface (CA = 109.1°) [59]. These contact and SA values for the PTFE- or PDMS-coated graphite surfaces are in significant contrast with the non-coated graphite surfaces, which have a static water CA of about 95 ± 2° and SA of over 90° as described in the previous section.

The improved surface hydrophobic property of the coated graphite surfaces should attributed to the surface roughness of

Table 3. *Wettability of silica particle/PDMS composite coatings on the graphite surface*[a].

Particle size (nm)		0[b]	72	262	510	745	1139
Silica particle/ PDMS-1[c]	CA	145 ± 5°	133 ± 5°	146 ± 3°	144 ± 3°	147 ± 3°	150 ± 2°
	SA	45 ± 5°	43 ± 5°	25 ± 3°	20 ± 2°	18 ± 2°	10 ± 3°
Silica particle/ PDMS-2[d]	CA	145 ± 5°	147 ± 3°	155 ± 2°	153 ± 3°	154 ± 3°	150 ± 2°
	SA	45 ± 5°	5 ± 2°	5 ± 2°	5 ± 2°	5 ± 2°	5 ± 2°

[a]Both CA and SA were measured with 10 μl water droplet.
[b]0 means only 1 wt% PDMS-1 (or PDMS-2) was used in coating formulation (without the particles).
[c]PDMS-1, hydroxyl-terminated PDMS.
[d]PDMS-2, Sylgard 184.

the original (non-coated) graphite surfaces. As showed in Figure 2a, the surface of non-coated graphite has considerable irregular features and its average roughness (Ra) is 4.23 μm (Figure 3a). When the graphite is coated with PDMS, its surface roughness does not change appreciably. The surface Ra is 3.95 μm (Figure 3b). This result suggests that the rough surface of graphite enhances the hydrophobicity with the PDMS coating. However, the water SA on PDMS-coated graphite is still high. In order to decrease this value and make water easily slide on the graphite surface, its surface roughness should be adjusted to an appropriate range. In the present work, silica particles were used to adjust the surface roughness.

3.3 Hydrophobic coating on the graphite surface with silica particle/PDMS-1 composite

The coatings of silica particle/PDMS-1 composite are first applied on the graphite surface, where PDMS-1 is hydroxyl-terminated PDMS. During the curing process, the hydroxyl groups, located in PDMS-1 and on silica particles, dehydrate and cross-link together by heating, to form the coating. PDMS works as a low surface energy matrix in the coating while the surface roughness is adjusted by the silica particles. After the curing, static CA and SA of water are measured on the coated graphite surface and given in Table 3. Compared with the graphite surface coated only with PDMS-1, the static CAs change insignificantly on the composite coatings, especially those with silica particles of sizes 262–745 nm. However, SAs decrease significantly with the coatings. For example, it is about 25° on graphite coated with 262 nm-sized silica particle/PDMS-1 composite. This value is already much lower than that on graphite coated with PDMS-1 only, where the SA is about 45°. As the particle size is increased to 745 nm, the SA is about 18° on the coating. Furthermore, when the particle size is about 1.139 μm, the SA decreases to about 10°. Water droplets could easily move on the composite-coated surface.

However, when the size of particles is as small as 72 nm, the water CA on the graphite surface coated by the silica particle/PDMS-1 composite is just 133 ± 5°, which is lower than that on graphite coated only with PDMS-1. Since the silica particles are synthesized from TEOS, their surfaces are full of hydroxyl groups. When the size of silica particles decreases, the overall density of hydroxyl groups is increased on the surface because of a greater surface area to volume ratio. On the other hand, the cure of PDMS in this silica particle/PDMS-1 composite is mainly due to dehydration among the hydroxyl groups of PDMS-1 and silica particles. Therefore, as the size of the silica particles is decreased to 72 nm, the increased hydroxyl groups on the surface are hard to be totally covered by the loaded hydroxyl-terminated PDMS.

In a control experiment, the concentration of PDMS-1 is increased to 1.5 wt% in the composite so that more PDMS-1 can be loaded on the surface and cover the silica particles. However, after 40 min curing at 180°C, some spots of the coating appear to be more shiny and thicker than the other places. The measured static CA decreases to 120°. This suggests that the increased loading of PDMS-1 leads to a thick PDMS-1 layer, which overwhelms the contribution of surface roughness to the surface hydrophobicity. Consequently, a reduced CA and hence reduced hydrophobicity result.

SEM images depict the surface topography of silica particle/PDMS-1 composite coatings (Figure 2b and c). When the graphite is coated with 262 nm-sized silica particle/PDMS-1 composite, quantities of silica particles fill in the pores on the graphite surface (Figure 2b). Although those particles are closely packed, they are still well dispersed on the surface, and their edges can easily be distinguished. The average surface roughness Ra of this coating is about 2.73 μm (Figure 3c), lower than that of graphite coated only by PDMS-1 (Ra, 3.95 μm). In addition, Rt (peak-to-valley distance) decreases to 34.14 μm on the composite coating compared with the value 150.64 μm on the graphite coated with PDMS-1 only. The large valleys on the surface seem to be filled by silica particles. Similar surface topography could also be seen on the coating with silica particles of size 1.139 μm (Figure 2d). On the basis of previous studies [60], much high surface roughness can enhance the static CA on the hydrophobic surface, but also increase the SA and weaken the movability of water on the surface. Here the adjusted surface roughness from the composite coating helps to lower down the SA on graphite.

3.4 Superhydrophobic coating on the graphite surface with silica particle/PDMS-2 composite

It requires 30 min to completely cure the coatings of silica particle/PDMS-1 composite. This period of time is long enough

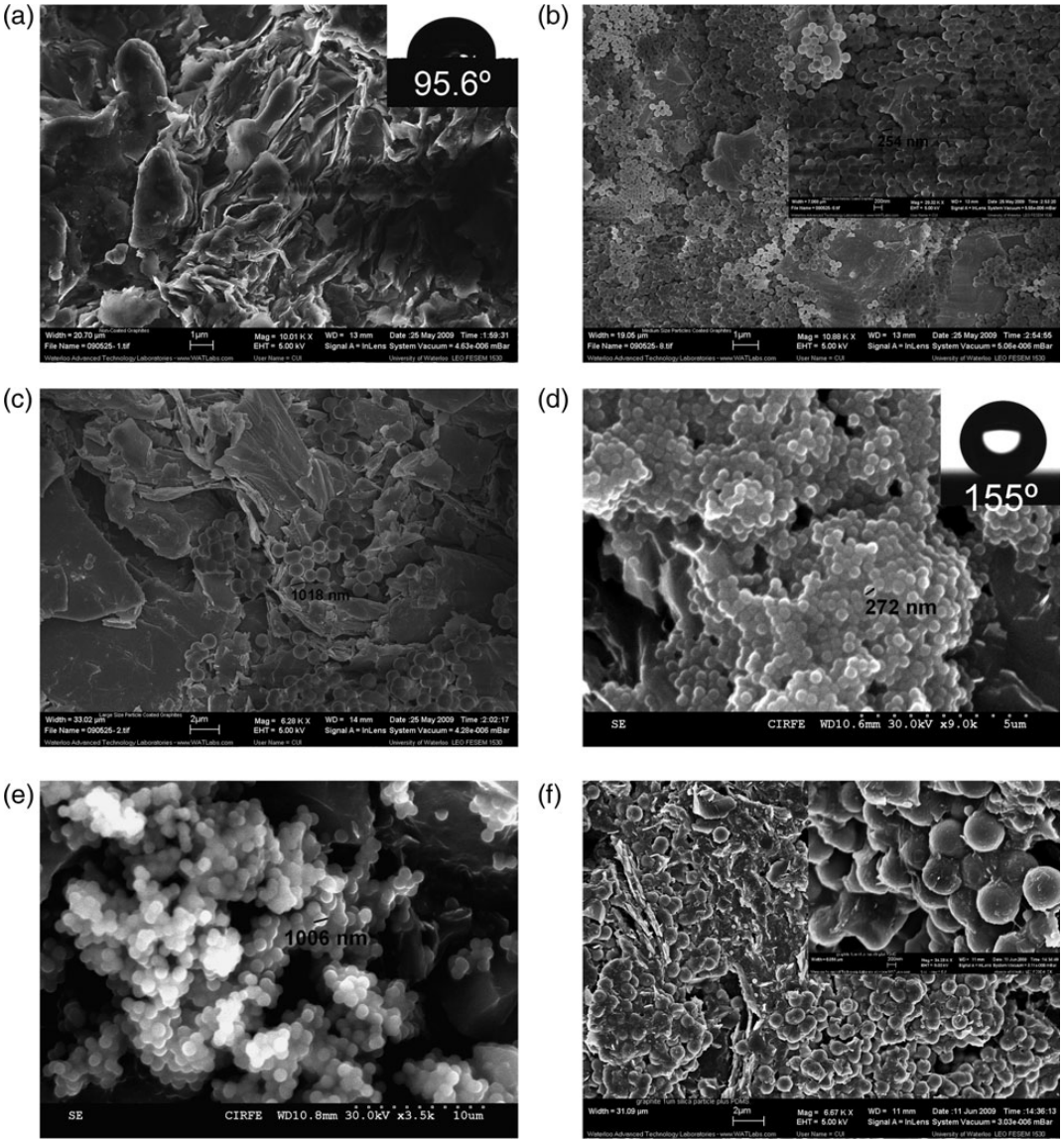

Figure 2. *SEM images showing the surface topography of graphite surface: (**a**) non-coated; (**b**) coated with 262 nm silica particle/PDMS-1 (hydroxyl terminated PDMS) composite; (**c**) coated with 1 μm silica particle/PDMS-1 composite; (**d**) coated with 262 silica particle/Sylgard 184 (PDMS-2) composite; (**e**) coated with 1 μm silica particle/PDMS-2 composite; (**f**) same coating as in (e) but treated with ultrasound for 1 h. The inserted images of (a) and (d) show the static CA of water, and inserted images of (b) and (f) show the detailed topography of coating.*

for PDMS-1 moving downwards to the bottom of silica particles before they were totally crosslinked. In other words, it is difficult to cure all the PDMS on the top surface of silica particles and provide a low surface energy protection there. However, it requires just 5 min to cure Sylgard 184 (PDMS-2) at 180°C, which can guarantee that more PDMS polymerization takes place on the top surface of silica particles. Therefore, PDMS-1 is replaced by PDMS-2 in the composite.

The static CA and SA on silica particle/PDMS-2 composite coatings are measured and listed in Table 3. It is obvious that these coatings have better water repellency than silica particle/PDMS-1 composite coatings. On a composite coating with 262 nm-sized silica particles, the CA is $155 \pm 2^\circ$ and SA is $5 \pm 2^\circ$. Decreasing the particle size to 72 nm, the CA is still about $147 \pm 3^\circ$ on the composite coating, higher than that on PDMS-1 involved coating. Increasing the particle size, even to 1.139 μm, the CAs and SAs show little difference on the composite coatings. These results suggest that the silica particle/PDMS-2 composite coatings can work with a wide range of particle sizes.

The advancing and receding CAs are also investigated on the silica particle/PDMS-2 composite coatings. Their difference, termed as CA hysteresis, is commonly used as a criterion for the sliding properties on the solid surface [59–63]. On graphite surfaces coated with 262 nm-sized silica particle/PDMS-2 composite, the advancing CA is $152.2 \pm 0.1^\circ$ and

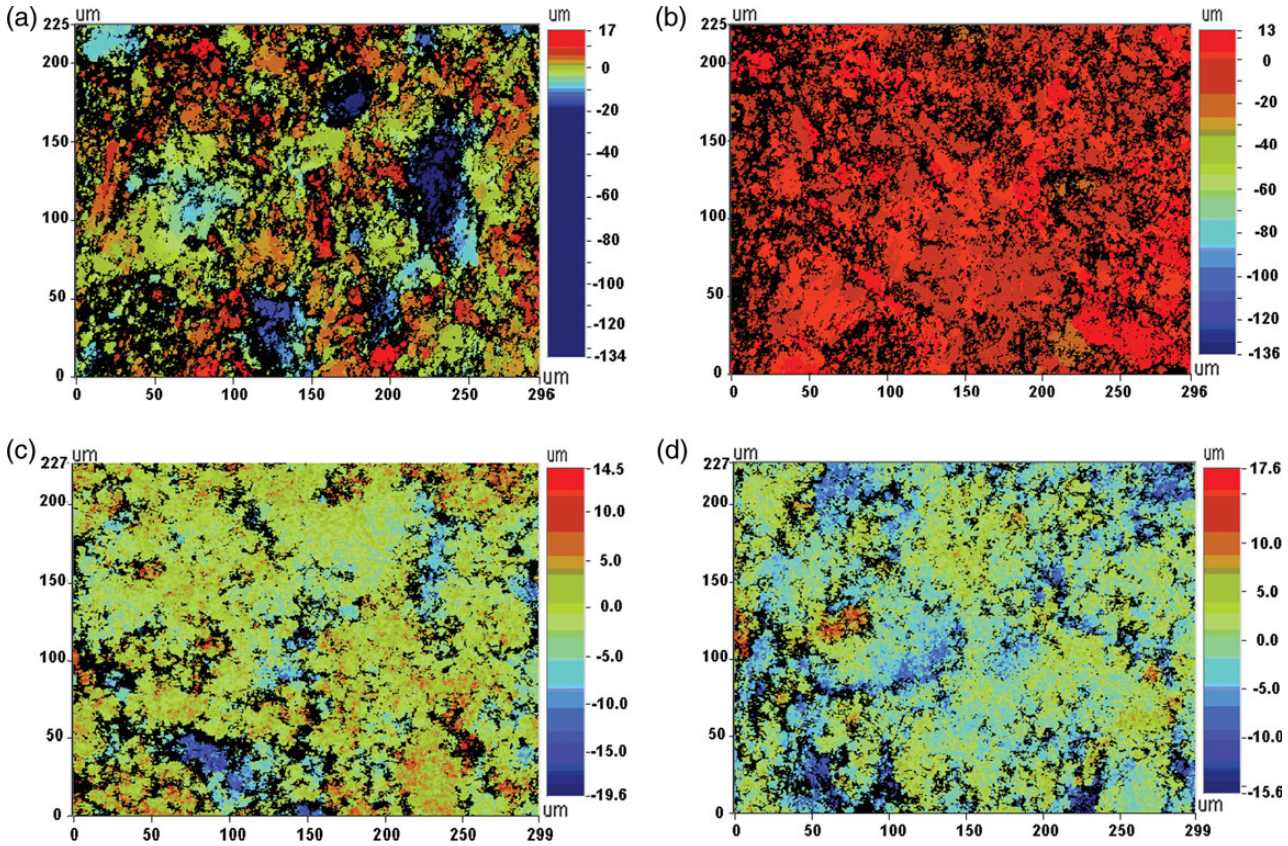

Figure 3. *Profilometry images showing the surface roughness of (**a**) non-coated graphite surface (Ra, 4.23 μm; Rt, 150.64 μm) and graphite coated with (**b**) hydroxyl-terminated PDMS (PDMS-1) (Ra, 3.95 μm; Rt, 148.76 μm), (**c**) 262 nm silica particle/PDMS-1 composite (Ra, 2.73 μm; Rt, 34.14 μm) and (**d**) 262 nm silica particle/Sylgard 184 (PDMS-2) composite (Ra, 2.85 μm; Rt, 33.23 μm).*

receding CA is $150.5 \pm 0.1^{\circ}$. The CA hysteresis is $1.7 \pm 0.1^{\circ}$. Additionally, when a water droplet of 10 μl is dropped to this coated surface (about 10 cm above the surface), the water droplet can bounce like an elastic ball on the surface. This is also related to the low CA hysteresis on the surface [64, 65].

3.5 Characterization of surface topography and roughness of composite coatings

Based on the previous studies [60], the surface wettablity is also related to the surface structure. In the present work, the surface topography of silica particle/PDMS-2 composite coating is characterized by SEM. When the graphite surface is coated with the 262 nm silica particle/PDMS-2 composite, the silica particles are aggregated together and show a caviar-like structure on the surface (Figure 2d), but not well separated on the surface like in the silica particle/PDMS-1 composite coating (Figure 2b). The similar topography is also observed with 1.139 μm silica particle/PDMS-2 composite coating (Figure 2e). This kind of surface structure is due to the fast curing of PDMS-2 in the composite coating. The PDMS-2 is cured not only on the top of silica particles, but also between the silica particles and linked them together. However, it is noticed that the surface configuration does not change the surface roughness significantly between the silica particle/PDMS-2 composite coating and silica particle/PDMS-1 composite coating. As graphite coated with the 262 nm silica particle/PDMS-2 composite, the Ra is 2.85 μm and Rt is 33.23 μm (Figure 3d). These values are almost the same with those of 262 nm silica particle/PDMS-1 composite coating, where the Ra is 2.73 μm and Rt is 34.14 μm (Figure 3c). A recent work shows that surface roughness reflects only the average parameter of the surface. Aside from the roughness, the surface configuration, like multiscale or hierarchical structures, also strongly influences the surface hydrophobicity, particularly the SA on the surface. It was reported that two-tiered structures, made up of superposition of two-scale (micro- and nano-) roughness patterns, may lead to the superhydrophobicity [39, 66–68]. The combination of micro- and nano-scaled structures can help to contort the gas–liquid–solid contact line, resulting in water droplet rolling on the surface. As to the coating of 262 nm silica particle/PDMS-2 composite, the silica particles adjust the surface roughness, resulting in the high static CA. Meanwhile, the nano-scaled silica particles aggregate together and form micro-scaled caviar-like structure on the graphite surface, and this two-tiered micro-/nano-structure further decreases the CA hysteresis, resulting in a lower SA on the surface.

Based on the aforementioned results, the superhydrophobic property of silica particle/PDMS-2 composite coatings is obtained for two main reasons: (i) the surface roughness and structure of graphite are adjusted by silica particles and (ii) the quick curing of PDMS-2 occurs in the composite coating. As to graphite, its surface is full of irregular pores and valleys. This heterogeneity cause a large CA hysteresis on the surface [61, 62], thus the water droplet is hard to slide on the surface. When graphite is coated with silica particle/PDMS-1 composite coating, the loaded silica particles decrease the surface heterogeneity of the graphite, resulted in decreasing SA on the surface. However, the curing time of PDMS-1 is long, and partial PDMS cannot be cured while on the top surface of this composite coating. In other words, PDMS is not significantly utilized in lowering the surface energy in this composite coating. In the case of silica particle/PDMS-2 composite coating, the short curing time of PDMS utilized the PDMS completely. Moreover, the quick curing of this composite also leads to the aggregation of silica particles and formation of two-tiered structure. Hence, the CA hysteresis is further decreased, resulting in more decrement in the SA.

3.6 Characteristics of two-phase flow through coated graphite channels

Figure 4 illustrates the typical water configuration while moving through the graphite single-flow channel for various channel surface coating (wettability) conditions, where water flows from left to right. The flow channel shown is made on a graphite plate with the top surface covered by a plexiglass for observation and visualization. For the channel shown in Figure 4a, the surfaces of graphite channel are not coated (the raw or original surface condition), and the liquid water seems to be continuous with a leading edge advancing towards the right and the main body of the liquid water wetting both the side and bottom graphite surfaces of the channel. For the channel shown in Figure 4b, the three graphite surfaces are coated with 262 nm-sized silica particles, and these surfaces are actually hydrophilic, while the top plexiglass is not coated and it is slightly hydrophilic. As a result of hydrophilic surface condition, liquid water spreads out on the bottom channel surface into the form of thin films, especially along the two corners between the side and bottom surfaces. In Figure 4b, the dark region on the left portion of the channel is the liquid film spreading on the bottom surface, and the light colour region on the right portion of the channel indicates that it is free of water film on the bottom surface; and the water film is spreading from the left to the right portion of the channel.

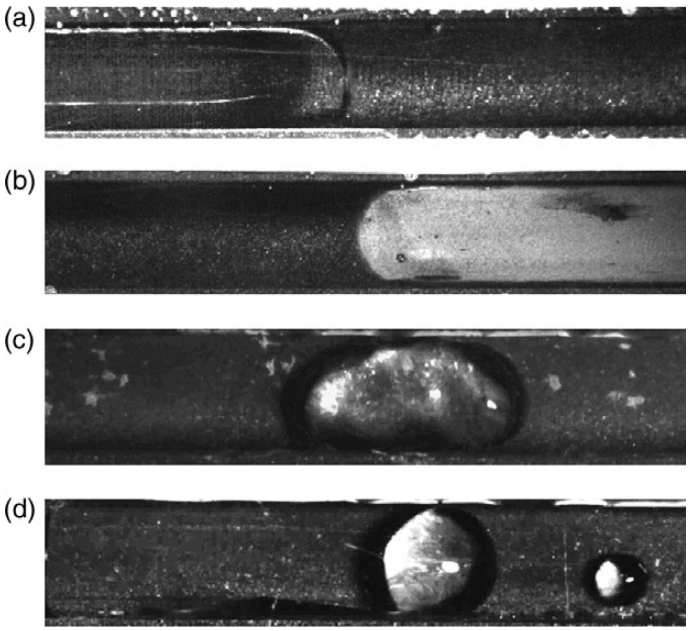

Figure 4. *Pictures showing the characteristics of water-air two-phase flow in a graphite channel with surfaces: (**a**) non-coated, (**b**) coated by 262 nm-sized silica particles, (**c**) coated by PTFE and (**d**) coated by 262 nm-sized silica particle/Sylgard 184 (PDMS-2) composite. The superficial velocity is 0.015 m/s for the liquid water and 4.81 m/s for the air flow in the channel. The water flow direction is from left to right.*

For the channel shown in Figure 4c, the three graphite surfaces are coated with PTFE, the conventional coating materials for PEMFC gas diffusion layers and catalyst layers for their hydrophobic surface condition, while the top plexiglass is still not coated. Since PTFE-coated surfaces are hydrophobic, but still with a fairly large SA of about 48°, liquid water in the channel is now contracted into an elongated drop (kind of potato shaped) while moving through the channel. Clearly, this water configuration is quite different from the cases shown in Figure 4a and b, demonstrating the effect of channel surface wettability on the water removal and transport through a flow channel.

For the channel shown in Figure 4d, the three graphite channel surfaces are coated with a 262 nm-sized silica particle/PDMS-2 composite, and the top plexiglass is still not coated. As pointed out earlier, the coated graphite surfaces in this case have a similar water CA as coated by PTFE shown in Figure 4c, but with a much smaller SA of about 5°. As a result, Figure 4d clearly shows that liquid water is almost in a spherical shape (the larger drop touches the two sides and the bottom surfaces while the smaller drop is only in contact with the bottom surface). In reality, the water droplets were seen rolled through the channel like solid balls. This significant change in the drop configuration between the PTFE-coated and silica particle/PDMS-2-coated channel surfaces is due to the considerable reduction in the SAs of the channel surfaces, and the small SA of about 5° indicates easy motion (removal) of liquid water over the solid surface.

The degree of easiness or difficulty for water transport or removal in the flow channel can also be illustrated by the pressure difference between the inlet and exit of the channel under a given flow condition, as shown in Figure 5. This is because the pressure drop is the primary driving force for the two-phase flow through the channel. Figure 5a shows the dry gas

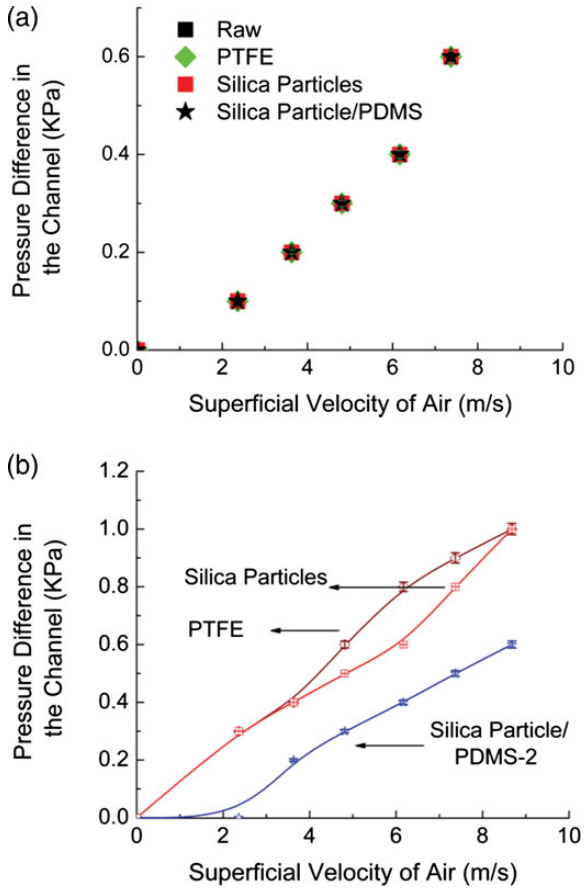

Figure 5. *Pressure difference between the inlet and the exit of the flow channels coated with PTFE, 262 nm silica particles and 262 nm silica particle/Sylgard 184 (PDMS-2) composite. The superficial velocity of water is (a) 0 m/s and (b) 0.015 m/s.*

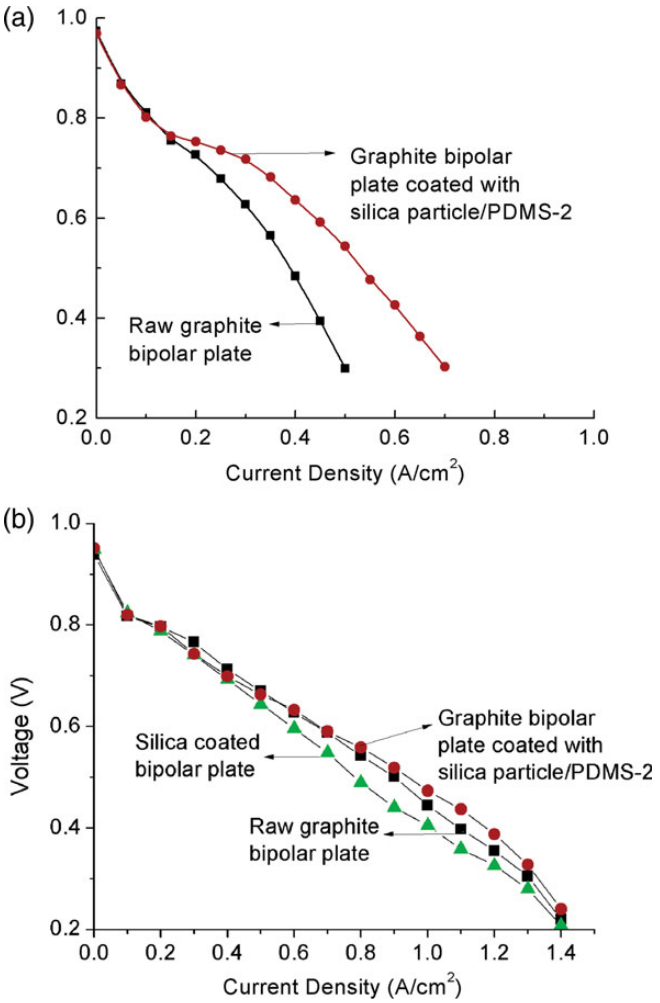

Figure 6. *Polarization curves showing the effect of flow channel surface wettability on the PEMFC performance. The anode flow channel is uncoated raw graphite surfaces, and the cathode flow channel surfaces are either uncoated raw graphite surfaces or coated with 262 nm-sized silica particle/PDMS-2 composite which is superhydrophobic with the CA of 155 ± 2° and SA of 5 ± 2°. (**a**) Both anode and cathode flow channels are single serpentine flow channel with a cross section of 3 mm × 3 mm; and cathode flow channel surface is coated as indicated in the figure; (**b**) both anode and cathode flow channels are three parallel serpentine flow channels with a cross section of 1 mm × 1 mm; and cathode flow channel surface is coated as indicated in the figure.*

pressure drop of the channels. Compared with non-coated graphite channel, the dry pressure drops in other coated channels do not show any differences. For all the results reported in Figure 5b, the superficial velocity of water is fixed at 0.015 m/s and the superficial velocity of air is varied as shown. For the channel surfaces (sides and bottom) coated by the silica particles, the surfaces are superhydrophilic with a CA of almost 0°. As a result, liquid advances quickly along the channel surfaces (especially the corner region) as mentioned earlier in association with Figure 4b; therefore, the pressure drop across the channel is mainly due to the reduction in the channel surface cross section.

However, for PTFE-coated channel surfaces those have large SAs, liquid water moves through the channel in a large blob in a potato-like shape, and hence has a fairly large resistance (or inertia) to motion. As a result, the pressure drop is also large, and in fact for the specific conditions of measurements shown in Figure 5b, it is even larger than the case with silica particle-coated superhydrophilic channel surfaces. However, for graphite channel surfaces coated by silica particle/PDMS-2 composite, which has a very small SA, the liquid water droplet is very easy to move over the channel surface with little driving force. As shown in Figure 5b, the pressure difference needed to drive the flow is very small, close to zero, for the superficial air velocity less than about 2 m/s. This is because the pressure gauge used in the experiment has a limited sensitivity and accuracy, and the nearly zero reading for the pressure difference represents the pressure drop is so small that the pressure gauge was not giving any noticeable readings. It is clear that silica particle/PDMS-2-coated channel yields the smallest pressure drop in the channel among the cases of surface coating investigated.

3.7 PEMFC performance test

The effect of flow channel surface wettability on the PEMFC performance has also been investigated as a confirmation of water management strategy through the channel surface coatings, as shown in Figure 6. The anode flow channels are not coated (raw or original graphite surfaces), while the cathode flow channel surfaces are coated with 262 nm-sized silica particle/PDMS-2 composite since this coating is most effective in removing water in the flow channel, as described earlier. Similar measurements are also conducted for cathode flow channel surfaces that are not coated (raw and original graphite surfaces) and coated with superhydrophilic coating (silica particles only) for comparison purpose. It is clear from Figure 6 that the PEMFC performance is improved significantly for the cathode flow channels coated with silica particle/PDMS-2 composite because of the small SA and easy water removal. For low current density region (<0.2 A/cm^2), the amount of liquid water produced, and hence required to be removed through the cathode flow channel, is low. As a result, there is no significant performance difference between the raw graphite channel and the coated superhydrophobic channel surfaces. However, for higher current densities, more liquid water is produced. The effect of water removal in the flow channel, hence, flow channel surface wettability, on the PEMFC performance becomes significant and increases with the current density.

It might be also pointed out that the results shown in Figure 6a was obtained when both anode and cathode flow channels were single serpentine flow channel with a cross section of 3 mm $\times$ 3 mm; and the cathode flow channel surface was coated as indicated in the figure; the results presented in Figure 6b were measured for both anode and cathode flow channels being three parallel serpentine flow channels with a cross section of 1 mm $\times$ 1 mm; and cathode flow channel surface coated as indicated in the figure. Clearly, the smaller flow channel size of 1 mm $\times$ 1 mm cross section yielded a much better performance as shown in the figures.

3.8 Stability of silica particle/PDMS-2 composite coatings

Aside from its hydrophobicity, the stability (or durability) of composite coatings is equally important to the applications of PEMFC since long lifetime is always desired. To determine the stability of the silica particle/PDMS-2 composite coating, coated graphite surfaces were immersed in Milli-Q (distilled or high purity) water in a shaker. The shaking rate was set at 40 rpm and temperature was controlled at 80°C. It is found that the static CA shows almost no changes, around 155° after 10 h shaking as shown in Figure 7. As to the SA, it could be kept lower than 10° in the first 6 h, and increases to 14° in the 10 h, but water droplets could still easily move on the graphite surface. PDMS is generally soft and flexible, and is cured under 180°C in experiment, thus its thermal stability will not be the concern in the application of the fuel cells. In the silica particle/PDMS-2 composite coating, the top layer of PDMS-2 cured from Sylgard 184 serves like a shield to cover and protect the silica particles beneath it on graphite. Since it is physical interaction between the PDMS-2 and silica particles in this composite coating, part of silica particles is still able to move. Hence, long-time shaking may lead to the movement of silica particles in the composite coating and resulting in the change of surface roughness. This is probably the reason for the change in water SA.

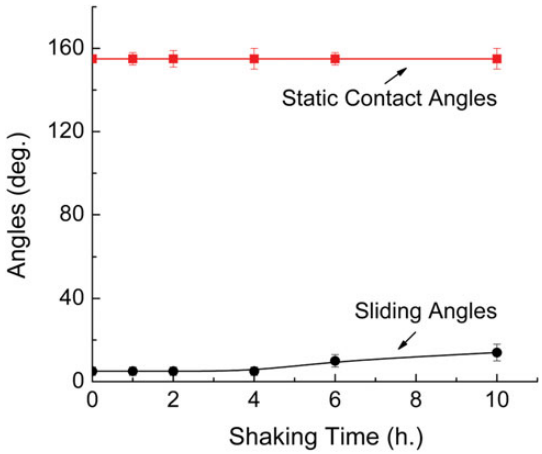

Figure 7. *Durability of the graphite surface coated with 262 nm-sized silica particle/Sylgard 184 (PDMS-2) composite through a shaking test. Shaking rate: 40 rpm; temperature: 80°C.*

In this study, graphite coated with the 1.139 μm silica particle/PDMS-2 composite was also tested with ultrasound. It was found that the surface static CA showed no changes and SA became even $<5°$ after the coated graphite was treated by ultrasound for 1 h. A water droplet of 5 μl could not stand on this surface, bounced and rolled off the surface directly. The SEM image (Figure 2f) shows that the shell of silica particle looks like cracked and some burrs grow on it, which should be caused by ultrasound. The new grown structures enrich the surface topography and then enhance the surface hydrophobic property.

4 CONCLUSIONS

In this study, the water management strategy in PEMFCs is investigated through the modification of flow channel wettability by various surface coatings. Different surface coating materials and techniques have been developed. It was found that graphite flow channel surfaces coated by the silica particle/PDMS (Sylgard 184) composite yields a superhydrophobic surface property with the CA of $155 \pm 2°$ and SA of $5 \pm 2°$, and a smallest pressure drop for the two-phase flow through the channel, indicating the easiest water removal from the channel. Therefore, such coated flow channels result in a significantly improved PEMFC performance. It was also found that such surface coating is fairly stable through shaking and ultrasound testing.

Acknowledgements

Financial support from the Natural Sciences and Engineering Research Council of Canada through a Strategic Projects Grant Supplemental Competition (Grant No.: STPSC 357087–07) and the Auto21 Networks of Centres of Excellence is gratefully acknowledged. The authors highly appreciate the Optikon Corporation Ltd. for their assistance in using their CMOS camera system for part of the study.

REFERENCES

[1] Barbir F. *PEM Fuel Cells. Theory and Practice. Academic Press* 2005, 95.
[2] Zhang FY, Wang XG, Wang CY. Liquid water removal from a polymer electrolyte fuel cell. *J Electrochem Soc* 2006;**153**:A225–32.
[3] Mench M. *Fuel Cell Engines*. Wiley, 2008.
[4] Kandlikar SG. Microscale and macroscale aspects of water management challenges in PEM fuel cells. *Heat Transfer Eng* 2008;**29**:575–87.
[5] Jiao K, Li X. Water transport in polymer electrolyte membrane fuel cells. *Progr Energ Combust Sci* 2011;**37**:221–91.
[6] Bazylak A. Liquid water visualization in PEM fuel cells: a review. *Int J Hydrogen Energy* 2009;**34**:3845–57.
[7] Li H, Tang Y, Wang Z, *et al*. A review of water flooding issues in the proton exchange membrane fuel cell. *J Power Sources* 2008;**178**:103–17.
[8] Dai W, Wang H, Yuan XZ, *et al*. A review on water balance in the membrane electrode assembly of proton exchange membrane fuel cells. *Int J Hydrogen Energy* 2009;**34**:9461–78.
[9] Owejan JP, Trabold TA, Jacobson DL, *et al*. Effects of flow field and diffusion layer properties on water accumulation in a PEM fuel cell. *Int J Hydrogen Energy* 2007;**32**:4489–502.
[10] Zhu W, Dunbar ZW, Masel RI. MicroCT X-ray imaging of water movement in a PEM fuel cell. *ECS Trans* 2008;**16**:995–1000.
[11] Bazylak A, Heinrich J, Djilali N, *et al*. Liquid water transport between graphite paper and a solid surface. *J Power Sources* 2008;**185**:1147–53.
[12] Natarajan D, Nguyen TV. Three-dimensional effects of liquid water flooding in the cathode of a PEM fuel cell. *J Power Sources* 2003;**115**:66–80.
[13] Liu X, Guo H, Ye F, *et al*. Flow dynamic characteristics in flow field of proton exchange membrane fuel cells. *Int J Hydrogen Energy* 2008;**33**:1040–51.
[14] Bourges-Monnier C, Shanahan MET. Influence of evaporation on contact angle. *Langmuir* 1995;**11**:2820–9.
[15] Li X, Sabir I. Review of bipolar plates in PEM fuel cells: flow field designs. *Int J Hydrogen Energy* 2005;**30**:359–71.
[16] Zhang X, Shi F, Niu J, *et al*. Superhydrophobic surfaces: from structural control to functional application. *J Mater Chem* 2008;**18**:621–33.
[17] Extrand CW. Relation between contact angle and the cross-sectional area of small, sessile liquid drops. *Langmuir* 2006;**22**:8431–34.
[18] Roach P, Shirtcliffe NJ, Newton MI. Progress in superhydrophobic surface development. *Soft Matter* 2008;**4**:224–40.
[19] Li XM, Reinhoudt D, Crego-Calama M. What do we need for a superhydrophobic surface? A review on the recent progress in the preparation of superhydrophobic surfaces. *Chem Soc Rev* 2007;**36**:1350–68.
[20] Feng XJ, Jiang L. Design and creation of superwetting/antiwetting surfaces. *Adv Mater* 2006;**18**:3063–78.
[21] Callies M, Quere D. On water repellency. *Soft Matter* 2005;**1**:55–61.
[22] Feng L, Li SH, Li YS, *et al*. Super-hydrophobic surfaces: from natural to artificial. *Adv Mater* 2002;**14**:1857–60.
[23] Neinhuis C, Barthlott W. Characterization and distribution of water-repellent, self-cleaning plant surfaces. *Ann Bot* 1997;**79**:667–77.
[24] Barthlott W, Neinhuis C. Purity of the sacred lotus, or escape from contamination in biological surfaces. *Planta* 1997;**202**:1–8.
[25] Kumbura EC, Sharpa KV, Mench MM. Liquid droplet behavior and instability in a polymer electrolyte fuel cell flow channel. *J Power Sources* 2006;**161**:333–45.
[26] Sinclair E, Kim SK, Akinleye HB, *et al*. Quantitation of gas-phase perfluoroalkyl surfactants and fluorotelomer alcohols released from nonstick cookware and microwave popcorn bags. *Environ Sci Technol* 2007;**41**:1180–5.
[27] Brook MA. *Silicon in Organic, Organometallic, and Polymer Chemistry*. Wiley, 1999, 256.
[28] Belorgey G, Sauvet G. Organosiloxane block and graft copolymers. In Johnes RG, Wataru A, Choinowski J (eds). *Silicon Containing Polymers: The Science and Technology of Their Synthesis and Applications*. Kluwer Academic Publishers, 2000, 70.
[29] Murase H, Fujibayashi T. Characterization of molecular interfaces in hydrophobic systems. *Prog Org Coat* 1997;**31**:97–104.
[30] Nosonovsky M, Bhushan B. Roughness-induced superhydrophobicity: a way to design non-adhesive surfaces. *J Phys Condens Matter* 2008;**20**:225009.
[31] Quéré D. Wetting and roughness. *Annu Rev Mater Res* 2008;**38**:71–99.
[32] Wenzel RN. Resistance of solid surfaces to wetting by water. *Ind Eng Chem* 1936;**28**:988–94.
[33] Cassie ABD, Baxter S. Wettability of porous surfaces. *Trans Faraday Soc* 1944;**40**:546–50.
[34] Gao L, McCarthy TJ. How Wenzel and Cassie were wrong. *Langmuir* 2007;**23**:3762–5.
[35] McHale G. Cassie and Wenzel: were they really so wrong? *Langmuir* 2007;**23**:8200–5.
[36] Marmur A, Bittoun E. When Wenzel and Cassie are right: reconciling local and global considerations. *Langmuir* 2009;**25**:1277–81.
[37] Wang S, Feng X, Yao J, *et al*. Controlling wettability and photochromism in a dual-responsive tungsten oxide film. *Angew Chem Int Ed* 2006;**45**:1264–67.
[38] Onda T, Shibuichi S, Satoh N, *et al*. Super-water-repellent fractal surfaces. *Langmuir* 1996;**12**:2125–7.
[39] Shibuichi S, Onda T, Satoh N, *et al*. Super water-repellent surfaces resulting from fractal structure. *J Phys Chem* 1996;**100**:19512.
[40] Tadanaga K, Katata N, Minami T. Formation process of super-water-repellent Al_2O_3 coating films with high transparency by the Sol-zGel method. *J Am Ceram Soc* 1997;**80**:3213–16.
[41] Tadanaga T, Morinaga J, Matsuda A, *et al*. Superhydrophobic–superhydrophilic micropatterning on flowerlike alumina coating film by the Sol–Gel method. *Chem Mater* 2000;**12**:590–2.
[42] Shiu J-Y, Kuo C-W, Chen P, *et al*. Fabrication of tunable superhydrophobic surfaces by nanosphere lithography. *Chem Mater* 2004;**16**:561–4.
[43] Qian B, Shen Z. Fabrication of superhydrophobic surfaces by dislocation-selective chemical etching on aluminum, copper, and zinc substrates. *Langmuir* 2005;**21**:9007–9.
[44] Wu Y, Sugimura H, Inoue Y, *et al*. Thin films with nanotextures for transparent and ultra water-repellent coatings produced from trimethylmethoxysilane by microwave plasma CVD. *Chem Vapor Deposition* 2002;**8**:47–50.
[45] Lau KKS, Bico J, Teo KBK, *et al*. Superhydrophobic carbon nanotube forests. *Nano Lett* 2003;**3**:1701–5.
[46] Feng L, Li S, Li H, *et al*. Super-hydrophobic surface of aligned polyacrylonitrile nanofibers. *Angew Chem Int Ed* 2002;**41**:1221–3.
[47] Li X, Chen G, Ma Y, *et al*. Preparation of a super-hydrophobic poly(vinyl chloride) surface via solvent–nonsolvent coating. *Polymer* 2006;**47**:506–9.

[48] Barbir F. *PEM Fuel Cells. Theory and Practice*. Academic Press, 2005, 100.
[49] Wang M, Woo K, Kim D, *et al*. Study on impregnation of polytetrafluoroethylene in graphite for use as fuel cell collector. *Int J Hydrogen Energy* 2005;**30**:1027–30.
[50] Taniguchi A, Yasuda K. Highly water-proof coating of gas flow channels by plasma polymerization for PEM fuel cells. *J Power Sources* 2005;**141**:8–10.
[51] Stöber AF, Bohn EJ. Controlled growth of monodisperse silica spheres in the micron size range. *J Colloid Interface Sci* 1968;**26**:62–8.
[52] Van B, Vrij A. Synthesis and characterization of monodisperse colloidal organo-silica spheres. *J Colloid Interface Sci* 1993;**156**:1–18.
[53] Jesionowski T, Siwińska-Stefańska K, Krysztafkiewicz A, *et al*. Characterization of TiO_2 surface following the modification with silane coupling agents. *Pol J Chem Technol* 2007;**9**:72–6.
[54] del Río OI, Neumann1 AW. Axisymmetric drop shape analysis: computational methods for the measurement of interfacial properties from the shape and dimensions of pendant and sessile drops. *J Colloid Interface Sci* 1997;**196**:136–47.
[55] Barreira SVP, Silva F. Surface modification chemistry based on the electrostatic adsorption of poly-*l*-arginine onto alkanethiol modified gold surfaces. *Langmuir* 2003;**19**:10324–31.
[56] Volpe CD, Siboni S. Comment on 'is a sessile drop in an atmosphere saturated with its vapor really at equilibrium?' and subsequent criticism. *Langmuir* 2006;**22**:5963–7.
[57] Kusumaatmaja H, Vrancken RJ, Bastiaansen CWM, *et al*. Anisotropic drop morphologies on corrugated surfaces. *Langmuir* 2008;**24**:7299–308.
[58] Ranjan R, Brittain WJ. Combination of living radical polymerization and click chemistry for surface modification. *Macromolecules* 2007;**40**:6217–23.
[59] Sheng X, Zhang J, Jiang L. Application of the restricting flow of solid edges in fabricating superhydrophobic surfaces. *Langmuir* 2009;**25**:9903–7.
[60] Liu K, Yao X, Jiang L. Recent development in bio-inspired special wettability. *Chem Soc Rev* 2010;**39**:3240–55.
[61] Johnson RE, Dettre RH. Contact angle hysteresis. I. study of an idealized rough surface. In Fowkes FM (ed). *Contact Angle, Wettability, and Adhesion*. American Chemical Society, 1964, 112–35.
[62] Dettre RH, Johnson RE. Contact angle hysteresis. II. Contact angle measurements on rough surfaces. In Fowkes FM (ed). *Contact Angle, Wettability, and Adhesion*. American Chemical Society, 1964, 136–44.
[63] Chen W, Fadeev AY, Hsieh MC, *et al*. Ultrahydrophobic and ultralyophobic surfaces: some comments and examples. *Langmuir* 1999;**15**:3395–9.
[64] Richard D, Clanet C, Quéré D. Surface phenomena: contact time of a bouncing drop. *Nature* 2002;**417**:811.
[65] Aussillous P, Quéré D. Liquid marbles. *Nature* 2001;**411**:924–7.
[66] Herminghaus S. Roughness-induced non-wetting. *Europhys Lett* 2000;**52**:165–70.
[67] Patankar NA. Mimicking the lotus effect: influence of double roughness structures and slender pillars. *Langmuir* 2004;**20**:8209–13.
[68] Yildirim Erbil H, McHale G, Newton MI. Drop evaporation on solid surfaces: constant contact angle mode. *Langmuir* 2002;**18**:2636–41.